Almost Global Three-Dimensional Path-Following Guidance Law for Arbitrary Curved Paths

Erlend M. Coates[1], Tarek Hamel[2] and Thor I. Fossen[3]

***Abstract*— Motivated by aircraft applications, we revisit the path-following guidance problem in three dimensions. First, by formulating the path-following error directly in the inertial frame, we propose a class of guidance laws for regular parameterized paths that, unlike most approaches existing in the literature, do not require the explicit construction of a path frame. Based on an inner-outer loop control paradigm, the guidance law generates a normal acceleration command that is normal to the flow-relative velocity vector (as the lift force). This allows for a natural decomposition of the desired vehicle acceleration for aerial vehicles in coordinated turns: tangential acceleration for airspeed control and normal acceleration for guidance generated through bank-to-turn maneuvers, i.e., by tilting the lift vector. By using cascade arguments, we show that the proposed design leads to almost global stability results and thus relaxes the set of feasible initial conditions compared to existing methods. The efficacy of the proposed guidance law is demonstrated in a simulation study.**

I. INTRODUCTION

Over the past decade, the evolution of hardware technology and control algorithms has propelled the widespread adoption of compact Unmanned Aerial Vehicles (unmanned aerial vehicles (UAVs)) across civil, commercial, and scientific domains [1].

In high-performance applications, the position of the UAV is typically controlled by either trajectory tracking or path-following algorithms [2]. Path following ensures the vehicle's position converges to and follows a desired geometric path without any temporal constraints [3].

Path-following algorithms take precedence over trajectory tracking in fixed-wing aircraft, owing to several key factors. Such aircraft's aerodynamic attributes and overall performance are closely tied to their air-relative velocity. Ensuring precise trajectory tracking under these circumstances can pose considerable challenges, mainly when dealing with small UAVs where wind velocity constitutes a significant portion of the air-relative velocity. A typical fixed-wing aircraft's inherent underactuated and nonminimum phase characteristics further accentuate this complexity. Adding to the rationale, a study referenced in [4] underscores the advantages of path-following over trajectory tracking. It unveils that path-following obviates the inherent performance limitations intrinsic to trajectory tracking for nonminimum phase systems.

Many path-following methods have appeared in the literature in the last three decades. We refer the reader to the recent review [5] for an in-depth treatment. The existing literature on the 3D path following, e.g. [6], [7], [8], solve the control problem by specifying a guidance law in terms of *normal acceleration*, normal to the (ground) velocity vector of the aircraft. However, the control of fixed-wing aircraft is better defined in terms of the air-relative velocity vector for the following reasons:

- Performance specifications (lift, drag, stall, efficiency, etc.) of fixed-wing aircraft are defined using airspeed. Therefore, the airspeed should be carefully monitored and controlled during flight.
- A fixed-wing aircraft in a coordinated turn generate normal accelerations by reorienting the lift force through a banking ("bank-to-turn") maneuver. The lift force is normal to the relative velocity.
- Decomposing the desired acceleration in components orthogonal to, and in the direction of, the relative velocity allows us to decouple the guidance from airspeed control.
- In many applications, the discrepancy between the two different normal accelerations is ignored. However, this difference can be significant for fixed-wing aircraft flying in the wind, resulting in disturbances that deteriorate the control performance. This is especially true for small UAVs, which often experience significant wind velocities compared to their relative-air velocities.

This paper proposes a class of guidance laws for almost-global path-following of any viable path in three dimensions, especially suited for fixed-wing aircraft. We employ an inner-outer loop control paradigm: In the outer loop, a desired heading vector (the velocity direction) is chosen that steers the vehicle toward the path. The control design is achieved using a simple line-of-sight (LOS)-like feedback law, and in contrast to most existing methods for 3D path following [3], [6], [7], [8], we do not require the definition of a moving coordinate frame attached to the path. The desired heading vector is converted to a *relative* heading vector by carefully considering the wind triangle. In the inner loop, a control law on the two-sphere achieves the desired relative heading by assigning the normal acceleration, *normal to the relative velocity* chosen as the natural control input for fixed-wing aircraft. The resulting closed-loop system is analyzed in a cascade manner to show the almost globally asymptotic

[1]Erlend M. Coates is with the Department of ICT and Natural Sciences, Norwegian University of Science and Technology, Ålesund, Norway erlend.coates@ntnu.no

[2]Tarek Hamel is with I3S, Université Côte d'Azur, CNRS, Sophia Antipolis, France thamel@i3s.unice.fr

[3]Thor I. Fossen is with the Department of Engineering Cybernetics, Norwegian University of Science and Technology, 7491 Trondheim, Norway thor.fossen@ntnu.no

stability of the equilibrium point. The effectiveness of the proposed approach is demonstrated in a simulation case study. The main contributions can be succinctly outlined as follows:

1) We propose a novel guidance law tailored to *arbitrary curved paths in 3D*, offering *almost global stability properties*. This distinguishes the proposed approach from existing studies, which often focus on specific path types like straight lines or circular paths or impose limited starting conditions.
2) The control input is the normal acceleration, *normal to the relative velocity*, making the proposed guidance law particularly suited for fixed-wing aircraft.
3) The control design and implementation circumvent the need for *path frames* such as Frenet-Serret or parallel transport frames leading to a simple and modular structure in conjunction with the cascade design approach.
4) Lastly, we establish a nexus between the proposed guidance law and the classical LOS guidance law in the 2D case to show that the approach elegantly generalizes LOS guidance to the 3D case.

The paper is organized as follows: The problem formulation is stated in Section II. Section III explains the derivation of the outer-loop guidance controller, which includes the desired relative heading and the feedback law driving the progression of the reference point on the desired path. The inner-loop heading control is discussed in Section IV, while Section V covers the stability analysis of the complete closed-loop system. Numerical simulation results are presented in Section VI. Section VII highlights some concluding remarks. Finally, the relationship between our proposed guidance law and the classical LOS guidance law in 2D is established in Appendix A.

II. Problem Formulation

A. Notation

Let $\mathbb{R}^n$ denote the n-dimensional Euclidean space with the standard basis $\{e_1, \ldots, e_n\}$ and Euclidean norm $\|x\|$. When $n = 1$, we denote the absolute value of x by $|x|$. The identity matrix of dimension $n \times n$ is denoted by I_n.

The set $S^2 \coloneqq \{x \in \mathbb{R}^3 \colon \|x\| = 1\}$ is the two-sphere embedded in $\mathbb{R}^3$. At a point $p \in S^2$, the tangent space of S^2 at p is $\mathrm{T}_p S^2 \coloneqq \{x \in \mathbb{R}^3 \colon p^\top x = 0\}$.

The set $B_2 \coloneqq \{x \in \mathbb{R}^3 \colon \|x\| \leq 2\}$ is the closed 3-ball of radius two. We denote the boundary of B_2 by $\partial B_2 \coloneqq \{x \in \mathbb{R}^3 \colon \|x\| = 2\}$.

Further, $\Pi_p \coloneqq I_3 - pp^\top$ is the projection onto $\mathrm{T}_p S^2$. For any $x \in \mathbb{R}^3$ and $p \in S^2$, $x = \Pi_p x + pp^\top x$. In terms of the cross product, $\Pi_p x = -p \times (p \times x)$.

Let $a \in \mathbb{R}^3$ denote an acceleration vector, and consider some $p \in S^2$. Then $\Pi_p a \in \mathrm{T}_p S^2$ is the normal acceleration, orthogonal to p, and $pp^\top a$ is the tangential acceleration, in the direction of p. Let $a = \dot{v}$ and $v = V\eta$ where $V > 0$ is the speed ($V = \|v\|$) and $\eta \in S^2$ is the direction of the velocity ($\eta = \frac{v}{\|v\|}$). From the product rule, $\dot{v} = V\dot{\eta} + \dot{V}\eta$. It follows that $\Pi_\eta a = V\dot{\eta}$ and $\eta\eta^\top a = \dot{V}\eta$.

Finally, $\bar{\mathrm{sat}}^\Delta(x)$ ($\Delta > 0, x \in \mathbb{R}^n$) denotes a sufficiently smooth vector-valued saturation function. A typical example can be constructed using the hyperbolic tangent function: $\bar{\mathrm{sat}}^\Delta(x) = \Delta \tanh(\|x\|/\Delta)x/\|x\|$.

B. Dynamical Model

We address the guidance problem by considering the vehicle's second-order kinematics. We use a simplified model in which the vehicle is treated as a point particle moving in a uniform, constant wind field:

$$\dot{\xi} = v = V_a \eta_a + v_w \tag{1}$$

$$\dot{\eta}_a = \frac{1}{V_a} a_a^\perp, \tag{2}$$

where the vehicle's position and velocity are represented by $\xi \in \mathbb{R}^3$ and $v \in \mathbb{R}^3$, respectively, and $v_w \in \mathbb{R}^3$ is the constant wind velocity, all expressed with respect to an inertial reference frame $\mathcal{F}_I = \{e_1, e_2, e_3\}$. By assuming that the ground speed $V = \|v\|$ is nonzero, the velocity vector v is split into its ground speed $V = \|v\|$ and heading vector $\eta = v/V \in S^2$. To account for the effects of wind on the vehicle's motion, we similarly rewrite the air-relative velocity $v_a = v - v_w$ as $V_a \eta_a$, with $V_a = \|v_a\|$ representing the airspeed and $\eta_a \in S^2$ is the air-relative heading vector. The normal acceleration, $a_a^\perp \in \mathrm{T}_{\eta_a} S^2$, is the control input for the path-following problem considered here. For airspeed control, we assume that there is an independent inner-loop control law that uses the thrust input that stabilizes V_a to the desired value V_a^d (typically constant) greater than the stall airspeed V_a^s. From now on, and without loss of generality, we assume that V_a is constant and $V_a \geq V_a^s > V_w$, with V_w the wind magnitude $\|v_w\|$.

C. Path-Following Control Problem

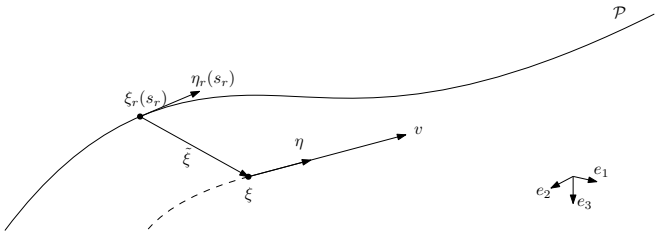

Fig. 1. Desired path.

Let the desired path be represented by a regular curve $\mathcal{P}$ in 3D space with a desired orientation, parameterized by signed arc length $s_r \in \mathbb{R}$ (s_r increases as the point on the path moves along the curve).

We denote a reference position on the path by $\xi_r(s_r) \in \mathbb{R}^3$, and the tangent vector at $\xi_r(s_r)$ by $\eta_r(s_r) \in S^2$. For regular curves, $\eta_r(s_r) = \partial\xi_r/\partial s_r$ is always well defined. The reference velocity (on the path) is then given by

$$\dot{\xi}_r = (\partial\xi_r/\partial s_r)\dot{s}_r = V_r \eta_r(s_r), \tag{3}$$

where $V_r \coloneqq \dot{s}_r$ is the "signed speed" on the path.

Let $\tilde{\xi} = \xi - \xi_r$ be the position error. From (1) and (3) it follows that

$$\dot{\tilde{\xi}} = v - V_r \eta_r(s_r) = V_a \eta_a + v_w - V_r \eta_r(s_r) \quad (4)$$

$$\dot{s}_r = V_r \quad (5)$$

As the regulation of V_a is ensured independently of the system under consideration, we can consider η_a and V_r as virtual controls to steer the vehicle towards the path and then follow the path onward in the direction of η_r by the asymptotic stabilization of the equilibrium $\tilde{\xi} = 0$. These key concepts are depicted in Fig. 1, which illustrates the main quantities involved in the control process.

We simplify the control design by dividing the path-following control problem into two subproblems:

1) Guidance that consists in defining η_a^d and V_r that ensure the asymptotic stabilization of $\tilde{\xi} = 0$ when $\eta_a \equiv \eta_a^d$ and consequently $V_r = V$.
2) Heading control that uses the normal acceleration $a_a^\perp$ to drive the actual direction η_a towards the desired direction η_a^d.

The resulting closed-loop system is then analyzed using cascaded dynamical systems theory.

For ease of notation, we denote $\eta_r(s_r)$ by η_r for the remainder of this paper.

III. Guidance controller Design

The guidance controller design is based on the model (4)–(5). By using η_a as virtual control and assigning an update law for V_r, one can impose the following dynamics $\dot{\tilde{\xi}} = f_1(\tilde{\xi}, s_r)$ for some function $f_1(\tilde{\xi}, s_r)$ such that for all t and s_r, $f_1(0, s_r) = 0$ and $\tilde{\xi}^\top f_1(\tilde{\xi}, s_r) < 0$ when $\tilde{\xi} \neq 0$. The global asymptotic (local exponential) stability proof of the origin $\tilde{\xi} = 0$ follows directly using the storage function $W_1(\tilde{\xi}) = (1/2)\|\tilde{\xi}\|^2$ along with standard Lyapunov stability arguments [9, Theorem 4.9]. Note however that $f_1(\tilde{\xi}, s_r)$ should be bounded, since from (4), $\|\Pi_{\eta_r}\dot{\tilde{\xi}}\| \leq V$ and hence precludes the global exponential stability of $\tilde{\xi} = 0$, which is consistent with the prior work on guidance in 2D [10].

Using the fact that V_r is a degree of freedom that can be used at will in the η_r direction, it is natural to rewrite $f_1 = f_1(\tilde{\xi}, s_r)$ in two components: one in the direction of η_r and the other in the orthogonal space: $f_1(\tilde{\xi}, s_r) = \Pi_{\eta_r} f_1(\tilde{\xi}, s_r) + \eta_r \eta_r^\top f_1(\tilde{\xi}, s_r)$.

At this stage, the virtual control input η_a^d and V_r enter into the equation via (4) using $\eta_a^d \equiv \eta_a$. The exact manner in which the virtual control input η_a^d and the input V_r enter imposes a class of feasible feedback $f_1(\tilde{\xi}, s_r)$ as discussed below.

A. Specifying the Progression of the Path Reference Point

Recalling (4) along with the fact that $\dot{\tilde{\xi}} = f_1(\tilde{\xi}, s_r)$ and pre-multiplying by $\eta_r^\top$ on both sides of the equation, one verifies that:

$$\eta_r^\top v - V_r \eta_r^\top \eta_r = \eta_r^\top f_1(\tilde{\xi}, s_r). \quad (6)$$

Since $\eta_r \in S^2$, one can rewrite (6) as follows:

$$V_r = \eta_r^\top v - \eta_r^\top f_1(\tilde{\xi}, s_r) = \eta_r^\top v - \eta_r^\top \left(\eta_r \eta_r^\top f_1(\tilde{\xi}, s_r)\right). \quad (7)$$

From there, one can choose the following feedback in the direction of η_r (or equivalently in the image of $\eta_r \eta_r^\top$):

$$\eta_r \eta_r^\top f_1(\tilde{\xi}, s_r) = -k_1 \eta_r \eta_r^\top \tilde{\xi}, \quad (8)$$

A saturated version of the form:

$$\eta_r \eta_r^\top f_1(\tilde{\xi}, s_r) = -\bar{\text{sat}}^{\Delta_1}\left(k_1 \eta_r^\top \tilde{\xi}\right) \eta_r, \quad (9)$$

with Δ_1 the saturation limit, is also a possible choice.

B. Specifying the Desired Heading Vector

To specify the desired relative heading vector η_a^d, we insert first the expression of V_r, (7), into (4) to get

$$\dot{\tilde{\xi}} = \Pi_{\eta_r} v + \eta_r \eta_r^\top f_1(\tilde{\xi}, s_r) = f_1(\tilde{\xi}, s_r). \quad (10)$$

By multiplying both sides of the above equation by Π_{η_r}, one arrives at the condition:

$$\Pi_{\eta_r}(V\eta) = \Pi_{\eta_r} f_1(\tilde{\xi}, s_r), \quad (11)$$

or equivalently,

$$\Pi_{\eta_r}(V_a \eta_a + v_w) = \Pi_{\eta_r} f_1(\tilde{\xi}, s_r). \quad (12)$$

From there, one has to select $\eta_a^d \in S^2$ to fulfill the objective. However, solving (12) for η_a can be challenging as it requires canceling the wind effect and ensuring normalization of $\eta_a \in S^2$. Therefore, to simplify this process, we will perform the assignment in two steps: 1) specify first η^d that satisfies (11) and then 2) transform η^d to η_a^d by involving the measure or an estimate of the wind according to (12). See the prior work [11] on how the wind can be estimated using standard sensors. We also refer the reader to the recent survey [12].

1) Desired heading η^d: The simplest choice for η^d is:

$$\eta^d = \frac{\eta_r - k_2 \Pi_{\eta_r} \tilde{\xi}}{\|\eta_r - k_2 \Pi_{\eta_r} \tilde{\xi}\|}, \quad (13)$$

with $k_2 > 0$. By referring to (11) and replacing η by the above expression of η^d, one verifies that $\Pi_{\eta_r} f_1(\tilde{\xi}, s_r) = -k_2 V \Pi_{\eta_r} \tilde{\xi} / \|\eta_r - k_2 \Pi_{\eta_r} \tilde{\xi}\|$. From there, one can consider the following option to independently manage the airplane's behavior in horizontal and vertical planes:

$$\eta^d = \frac{\eta_r - (k_2 \Pi_{e_3} + k_3 e_3 e_3^\top) \Pi_{\eta_r} \tilde{\xi}}{\|\eta_r - (k_2 \Pi_{e_3} + k_3 e_3 e_3^\top) \Pi_{\eta_r} \tilde{\xi}\|}, \quad (14)$$

in which case

$$\Pi_{\eta_r} f_1(\tilde{\xi}, s_r) = -\frac{V \Pi_{\eta_r} (k_2 \Pi_{e_3} + k_3 e_3 e_3^\top) \Pi_{\eta_r} \tilde{\xi}}{\|\eta_r - (k_2 \Pi_{e_3} + k_3 e_3 e_3^\top) \Pi_{\eta_r} \tilde{\xi}\|}, \quad (15)$$

with $k_3 > 0$. One verifies that if $k_3 = k_2$, (14) reduces to (13).

Remark 1: The expressions (13) and (14) are closely related to the classical *line-of-sight guidance laws* in 2D [10], see Appendix A for further details.

Similarly to (9) saturation functions can be introduced in the design of η^d to limit the maximum approach angle (w.r.t. η_r) when $\Pi_{\eta_r} \tilde{\xi}$ is large.

2) Desired relative heading η_a^d: To convert the desired heading vector to a desired *relative* heading vector, we will carefully consider the *wind triangle*.

Consider the wind triangle relating the velocity vector v, the air-relative velocity v_a and the wind velocity v_w:

$$v_a = v - v_w, \tag{16}$$

or equivalently:

$$V_a \eta_a = V\eta - v_w. \tag{17}$$

Dividing by V_a gives the following expression for the relative heading vector as a function of V, η, V_a, and the wind velocity v_w:

$$\eta_a = \frac{V}{V_a}\eta - \frac{v_w}{V_a}. \tag{18}$$

From geometrical considerations (see Fig. 2), one directly derives the following expression for the actual ground speed V as a function of V_a, η and v_w:

$$V = \eta^\top v_w + \sqrt{(\eta^\top v_w)^2 + V_a^2 - V_w^2}. \tag{19}$$

From there, one defines the expression for the desired relative heading:

$$\eta_a^d = \frac{V_d}{V_a}\eta^d - \frac{v_w}{V_a}. \tag{20}$$

with

$$V_d = v_w^\top \eta^d + \sqrt{(v_w^\top \eta^d)^2 + V_a^2 - V_w^2}. \tag{21}$$

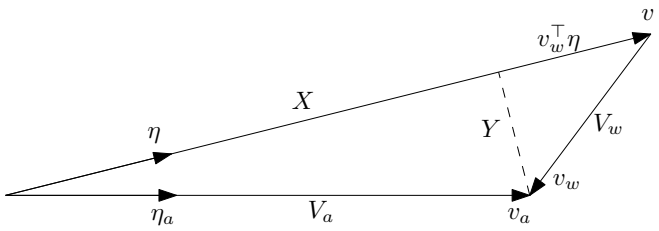

Fig. 2. The wind triangle. From the Pythagorean theorem, $Y = \sqrt{V_w^2 - (v_w^\top \eta)^2}$ and $X = \sqrt{(v_w^\top \eta)^2 + V_a^2 - V_w^2}$. Finally, $V = v_w^\top \eta + X$ to derive (19)

It is straightforward to verify by direct computation of $\|\eta_a^d\|$ that η_a^d is a unit vector and V_d is the normalizing factor required to compensate for v_w in (12). In particular, by inserting $\eta_a \equiv \eta_a^d$ with η_a^d defined by (20) into (12) one arrives at $\Pi_{\eta_r}\left(V_d \eta^d\right) = \Pi_{\eta_r} f_1(\tilde{\xi}, s_r)$. Finally, one notes that when $v_w = 0$, $\eta_a^d = \eta^d$.

IV. Heading Control

In this section, we address the (relative) heading control problem by formulating a control law for normal acceleration $a_a^\perp$ (2) to ensure that the actual relative heading vector η_a asymptotically tracks the desired heading vector η_a^d.

Since the heading vector η_a is an element of the two-sphere S^2, it is straightforward to verify that the normal acceleration $a_a^\perp \in \mathrm{T}_{\eta_a} S^2$ is an element of the tangent space at η_a.

Several control laws for systems evolving on the two-sphere S^2 can be found in the literature, e.g. [13], [14], [15], [8]. We propose to use the following:

Proposition 1: Consider the system (2) and a desired relative heading vector $\eta_a^d \in S^2$. Choose the following expression for $a_a^\perp$:

$$a_a^\perp = V_a^2 k_\eta \Pi_{\eta_a} \eta_a^d + V_a \eta_a \times \left(\dot{\eta}_a^d \times \eta_a^d\right), \quad k_\eta > 0. \tag{22}$$

Then,

1) the relative heading vector η_a converges either to η_a^d or $-\eta_a^d$.
2) the desired equilibrium $\eta_a = \eta_a^d$ is almost globally asymptotically stable and locally exponentially stable, uniformly in t_0.
3) the undesired equilibrium $\eta_a = -\eta_a^d$ is unstable.

Proof:

Let $\tilde{\eta}_a := \eta_a - \eta_a^d \in B_2$ denote the relative heading tracking error and consider the storage function given by

$$W_2(\tilde{\eta}_a) = \frac{1}{2}\tilde{\eta}_a^\top \tilde{\eta}_a = 1 - \eta_a^\top \eta_a^d. \tag{23}$$

One verifies that the time derivative of $W_2(\tilde{\eta}_a)$ is:

$$\dot{W}_2(\tilde{\eta}_a) = \tilde{\eta}_a^\top \dot{\tilde{\eta}}_a = -V_a k_\eta \eta_a^{d^\top} \Pi_{\eta_a} \eta_a^d \tag{24}$$

$$= -V_a k_\eta \|\eta_a \times \eta_a^d\|^2 \leq 0. \tag{25}$$

The stated properties in the proposition then follows from standard Lyapunov arguments, see e.g. [16, Proposition 1]. ∎

Remark 2: Since S^2 is a compact manifold, almost global asymptotic stability is the strongest stability result possible using continuous feedback [17]. However, global asymptotic stability can be achieved using hybrid control, where hysteresis-based switching ensures that *all* trajectories converge to the desired equilibrium [18], [19], [20], [21].

V. Analysis of the Complete Closed-Loop System

Proposition 2 (Main Result): Consider the second-order kinematics (1)–(2) under the control (22) with the desired relative heading η_a^d defined by (20) along with (21), and η^d satisfying (11), and V_r given by (7). Then, the equilibrium point $(\tilde{\xi}, \tilde{\eta}_a) = (0, 0)$ is almost globally asymptotically stable and locally exponentially stable with a basin of attraction including at least all initial conditions such that $\tilde{\eta}_a(0) < 2$.

Proof: To simplify the analysis, we consider the closed-loop system along the solutions $s_r(t)$ of (5), which lets us analyze the system as a cascade. The rigorous foundation that allows us to do this can be found in [22] and is based on the notion of *forward completeness* [23], which can easily be shown to hold for our system considered here.

Following the developments of Section III and substituting $\tilde{\eta}_a = \eta_a - \eta_a^d$ then leads to

$$\dot{\tilde{\xi}} = f_1(\tilde{\xi}, s_r(t)) + V_a \Pi_{\eta_r} \tilde{\eta}_a. \tag{26}$$

By construction, the origin $\tilde{\xi} = 0$ of the unperturbed system $\dot{\tilde{\xi}} = f_1(\tilde{\xi}, s_r(t))$ is uniformly globally asymptotically (locally exponentially) stable. Further, the perturbation term $V_a \Pi_{\eta_r} \tilde{\eta}_a$

is bounded, since $\tilde{\eta}_a \in B_2$. Moreover, from Proposition 1, we know that for all initial conditions except the (zero measure) set where $\|\tilde{\eta}_a\| = 2$, $\tilde{\eta}_a$ is converging (ultimately exponentially) to zero. Thus the integral $\int_{t_0}^{\infty} \|\tilde{\eta}_a(t)\| dt$ is bounded $\forall \tilde{\eta}_a(0) < 2$. By standard cascade arguments, e.g. [24, Theorem 2.1], with a minor technicality being that $\tilde{\eta}_a$ belongs to the compact space B_2, one concludes that the equilibrium point $(\tilde{\xi}, \tilde{\eta}_a) = (0, 0)$ is almost globally asymptotically stable, and locally exponentially stable. ■

VI. Simulation Results

In this section, we consider a simulation scenario to demonstrate the effectiveness of the proposed guidance law.

The specific choice of feedback used are given by (9) and (13) with the following set of control parameters: $k_1 = 20$, $\Delta_1 = 50$, $k_2 = 0.01$, and $k_\eta = 0.025$. Further, the simulation has been set up with $V_a = 18\,\mathrm{m\,s^{-1}}$ and $v_w = [10\,\mathrm{m\,s^{-1}}, 0, 0]^\top$. The desired path is the arc length parameterization of a helix of radius $R = 200\,\mathrm{m}$ and vertical separation $h = 100\,\mathrm{m}$:

$$\xi_r(s_r) = \begin{bmatrix} R\cos(\frac{s_r}{\sqrt{R^2+c^2}}) \\ R\sin(\frac{s_r}{\sqrt{R^2+c^2}}) \\ \frac{c}{\sqrt{R^2+c^2}} s_r \end{bmatrix}, \tag{27}$$

where $c = h/(2\pi)$. The initial conditions used are $\xi(t_0) = [0, 0, 0]^\top$ (in the center of the helix) and $\eta_a(t_0) = [-1, 0, 0]^\top$, resulting in a large initial heading error.

The simulation results are shown in Figs. 3–6 and show that after an initial transient, perfect path following is achieved, even for a very large initial heading error.

Fig. 3 shows how the vehicle (red) starts in the center of the helix and then converges to the path. In the bottom of Fig. 4, the angle θ between η_a and η_a^d is shown to converge rapidly to zero after an initial error of around 150 degrees. The "cross-track error" $\|\Pi_{\eta_r}\tilde{\xi}\|$ (middle) seemingly converges linearly to zero because the vehicle moves towards the path with a constant airspeed V_a. The bump in the magnitude of the normal acceleration (top) occurring around 30 sec is also seen in Fig. 5 and is caused by the wind. As the vehicle moves along the helix with constant airspeed, the ground speed V varies, depending on the angle of the velocity inertial direction with respect to the non-zero wind. One also observes that when $\tilde{\xi}$ converges close to zero, η is mostly aligned with η_r (see Fig. 6 that shows the time evolution of spherical coordinates of these vectors) and V_r converges to V. From Fig. 6 one also observes that there is an offset between η_a^d and η^d to account for the wind, while η_a converges to η_a^d, and η to η_d (and in turn, to η_r), respectively.

VII. Conclusions

This work introduces a novel class of path-following guidance laws endowed with almost-global asymptotic and local exponential stability for any feasible curved path in 3D. By directly defining the path-following error in the inertial frame, we show that the definition of an explicit 'path frame' moving along the path is not required. In a cascade approach, we establish conditions for selecting suitable feedback laws.

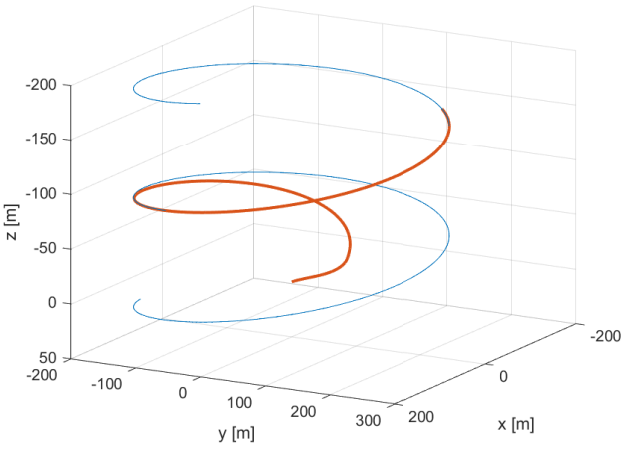

Fig. 3. Path following of helical path. Desired path $\mathcal{P}$ in blue, and the path traced out by the vehicle in red. The direction of travel is upwards.

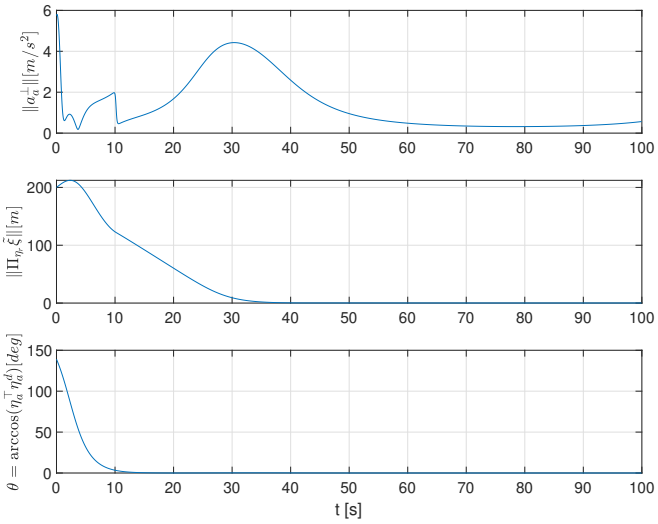

Fig. 4. From top to bottom: the magnitude of normal acceleration (normal to η_a), the magnitude of the orthogonal component of the position error, and the angle between desired and actual relative heading.

Furthermore, by choosing the normal acceleration, the vector orthogonal to the relative velocity as the control input makes, we show that this guidance law is particularly well-suited for fixed-wing aircraft. Simulation results are provided to demonstrate the effectiveness of the proposed method.

Appendix

A. Relation to Classical Line-of-Sight Guidance Laws Using Angles

Let parameterizations of η_r and η^d based on the commonly used spherical coordinates be given by:

$$\eta_r = \begin{bmatrix} \cos(\gamma_r)\cos(\chi_r) \\ \cos(\gamma_r)\sin(\chi_r) \\ -\sin(\gamma_r) \end{bmatrix}, \quad \eta^d = \begin{bmatrix} \cos(\gamma_d)\cos(\chi_d) \\ \cos(\gamma_d)\sin(\chi_d) \\ -\sin(\gamma_d) \end{bmatrix} \tag{28}$$

where the pairs χ_r, γ_r and χ_d, γ_d are the azimuth and elevation angles of η_r, η^d, respectively.

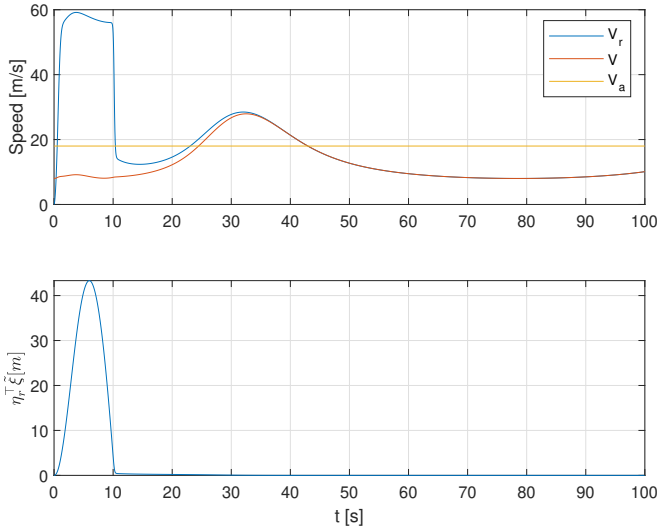

Fig. 5. Top: V_r converges to V as the component of $\tilde{\xi}$ in the direction of η_r (bottom) goes to zero and η is aligned with η_r. V_a can be seen to be constant.

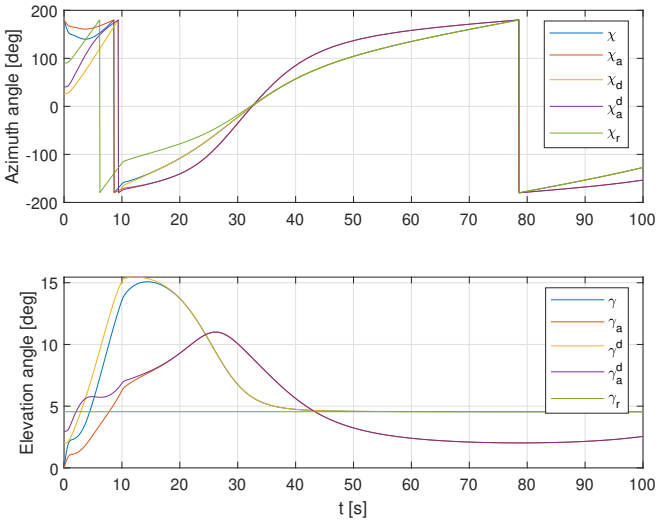

Fig. 6. Azimuth and elevation angles. For each respective vector, the azimuth angle is $\chi_* = \text{atan2}(e_2^\top \eta_*, e_1^\top \eta_*)$, and the elevation angle is $\gamma_* = \arcsin(-e_3^\top \eta_*)$.

We can derive a relation between the guidance laws (13)–(14) and the classical angle-based line-of-sight (LOS) guidance laws in 2D (e.g. [3], [10]) by projecting to the horizontal plane using the projection matrix Π_{e_3}. The projection is illustrated in Fig. 7. By considering the projection of the right triangle made up by η^d and its components in the direction of, and orthogonal to η_r, Equations (13) and (14) can be expressed in terms of azimuth (course) angles as

$$\chi_d = \chi_r + \arctan\left(\frac{-k_2 y_e}{\cos(\gamma_r)}\right), \quad \gamma_r \neq \pm\frac{\pi}{2} \tag{29}$$

where y_e is the *cross-track error*, i.e. the horizontal component of $\Pi_{\eta_r}\tilde{\xi}$, given by $y_e \coloneqq (\Pi_{\eta_r}\tilde{\xi})^\top (e_3 \times \eta_r)^\top / \|e_3 \times \eta_r\|$. The expression (29) is equivalent to that given in [3], [10] with $\Delta = \cos(\gamma_r)/k_2$. The control laws (13)–(14) thus

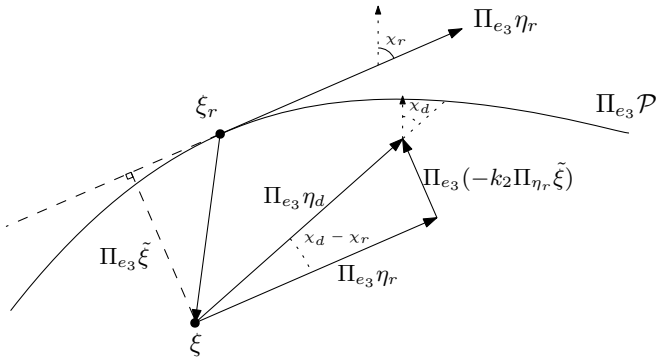

Fig. 7. Projection to the horizontal plane. The magnitude of $\Pi_{e_3}\eta_r$ equals $\cos(\gamma_r)$, and $\|\Pi_{e_3}\Pi_{\eta_r}\tilde{\xi}\| = |y_e|$.

provide natural generalizations of 2D LOS guidance laws to 3D using unit vectors in S^2.

References

[1] R. W. Beard and T. W. McLain, *Small Unmanned Aircraft*. Princeton, NJ: Princeton University Press, 2012.

[2] A. P. Aguiar and J. P. Hespanha, "Trajectory-tracking and path-following of underactuated autonomous vehicles with parametric modeling uncertainty," *IEEE Transactions on Automatic Control*, vol. 52, no. 8, pp. 1362–1379, 2007.

[3] M. Breivik and T. Fossen, "Principles of guidance-based path following in 2d and 3d," in *Proceedings of the 44th IEEE Conference on Decision and Control*, 2005.

[4] A. Aguiar, J. Hespanha, and P. Kokotovic, "Path-following for non-minimum phase systems removes performance limitations," *IEEE Transactions on Automatic Control*, vol. 50, no. 2, pp. 234–239, 2005.

[5] N. Hung, F. Rego, J. Quintas, J. Cruz, M. Jacinto, D. Souto, A. Potes, L. Sebastiao, and A. Pascoal, "A review of path following control strategies for autonomous robotic vehicles: Theory, simulations, and experiments," *Journal of Field Robotics*, 2022.

[6] N. Cho, Y. Kim, and S. Park, "Three-dimensional nonlinear differential geometric path-following guidance law," *Journal of Guidance, Control, and Dynamics*, vol. 38, no. 12, pp. 2366–2385, 2015.

[7] V. Cichella, I. Kaminer, V. Dobrokhodov, E. Xargay, N. Hovakimyan, and A. Pascoal, "Geometric 3d path-following control for a fixed-wing UAV on SO(3)," in *AIAA Guidance, Navigation, and Control Conference*. American Institute of Aeronautics and Astronautics, jun 2011.

[8] J.-M. Kai, T. Hamel, and C. Samson, "A unified approach to fixed-wing aircraft path following guidance and control," *Automatica*, vol. 108, p. 108491, 2019.

[9] H. K. Khalil, *Nonlinear Systems, 3rd ed.* Prentice-Hall, 2002.

[10] T. I. Fossen and K. Y. Pettersen, "On uniform semiglobal exponential stability (USGES) of proportional line-of-sight guidance laws," *Automatica*, vol. 50, no. 11, pp. 2912–2917, 2014.

[11] T. A. Johansen, A. Cristofaro, K. Sorensen, J. M. Hansen, and T. I. Fossen, "On estimation of wind velocity, angle-of-attack and sideslip angle of small UAVs using standard sensors," in *2015 International Conference on Unmanned Aircraft Systems (ICUAS)*, 2015.

[12] P. Tian, H. Chao, M. Rhudy, J. Gross, and H. Wu, "Wind sensing and estimation using small fixed-wing unmanned aerial vehicles: A survey," *Journal of Aerospace Information Systems*, vol. 18, no. 3, pp. 132–143, 2021.

[13] F. Bullo, R. Murray, and A. Sarti, "Control on the sphere and reduced attitude stabilization," *IFAC Proceedings Volumes*, vol. 28, no. 14, pp. 495–501, 1995.

[14] N. Chaturvedi, N. McClamroch, and D. Bernstein, "Asymptotic smooth stabilization of the inverted 3-d pendulum," *IEEE Transactions on Automatic Control*, vol. 54, no. 6, pp. 1204–1215, 2009.

[15] P. Corke and R. Mahony, "Sensing and control on the sphere," in *Springer Tracts in Advanced Robotics*. Springer Berlin Heidelberg, 2011, pp. 71–85.

[16] E. M. Coates and T. I. Fossen, "Geometric reduced-attitude control of fixed-wing UAVs," *Applied Sciences*, vol. 11, no. 7, p. 3147, 2021.

[17] S. P. Bhat and D. S. Bernstein, "A topological obstruction to continuous global stabilization of rotational motion and the unwinding phenomenon," *Systems & Control Letters*, vol. 39, no. 1, pp. 63–70, 2000.

[18] C. G. Mayhew and A. R. Teel, "Global stabilization of spherical orientation by synergistic hybrid feedback with application to reduced-attitude tracking for rigid bodies," *Automatica*, vol. 49, no. 7, pp. 1945–1957, 2013.

[19] T. Lee, "Optimal hybrid controls for global exponential tracking on the two-sphere," in *2016 IEEE 55th Conference on Decision and Control (CDC)*, 2016.

[20] P. Casau, C. G. Mayhew, R. G. Sanfelice, and C. Silvestre, "Robust global exponential stabilization on the n-dimensional sphere with applications to trajectory tracking for quadrotors," *Automatica*, vol. 110, p. 108534, 2019.

[21] D. Reinhardt, E. M. Coates, and T. A. Johansen, "Hybrid control of fixed-wing UAVs for large-angle attitude maneuvers on the two-sphere," *IFAC-PapersOnLine*, vol. 53, no. 2, pp. 5717–5724, 2020.

[22] A. Loria, "From feedback to cascade-interconnected systems: Breaking the loop," in *2008 47th IEEE Conference on Decision and Control*, 2008.

[23] D. Angeli and E. D. Sontag, "Forward completeness, unboundedness observability, and their lyapunov characterizations," *Systems & Control Letters*, vol. 38, no. 4-5, pp. 209–217, 1999.

[24] A. Loría and E. Panteley, "Cascaded nonlinear time-varying systems: Analysis and design," in *Advanced Topics in Control Systems Theory*. Springer London, 2005, pp. 23–64.